Progress In Electromagnetics Research Letters, Vol. 30, 153–162, 2012

SPECTRO-TEMPORAL MISMATCH ANALYSIS OF A TRANSMISSION LINE BASED ON ON-WAFER OPTICAL SAMPLING

D.-J. Lee*, J.-Y. Kwon, and J.-G. Lee

Center for Electromagnetic Wave, Korea Research Institute of Standards and Science, 209 Gajeong-Ro, Yuseong-gu, Daejeon 305-340, Korea

Abstract—We present an optical sampling technique that enables exploration of mismatches of a microstrip transmission line based on reflection analyses of electromagnetic pulses. The external electro-optic sampling scheme with a minute crystal detects high-speed electrical pulses over arbitrary locations of a line with very low-intrusiveness. The temporal pulsed signals measured with an on-wafer optical probing system and the corresponding spectra are obtained to analyze the transfer characteristics of a microstrip transmission line with 20 GHz bandwidth. The spectro-temporal response was cross-checked with commercial instruments. Applications of this optical probing technique to explore mismatches at the terminal port — based on both time and frequency domain reflectometry analyses — are also presented.

1. INTRODUCTION

The sampling oscilloscope system for the time domain display of high-speed pulsed signals provides a more intuitive look at microwave devices than frequency domain analysis because it gives a direct and obvious view of the locations and magnitudes of each discontinuity as a function of time or distance. Although commercial vector network analyzers (VNAs) can also provide time domain analysis, they measure frequency-dependant complex arrays (S-parameters) by making swept frequency measurements in the spectral band of interest and mathematically transforming the data into a time domain. Such a technique inherently contains artifacts that cannot be completely

Received 5 December 2011, Accepted 14 March 2012, Scheduled 21 March 2012

* Corresponding author: Dong-Joon Lee (dongjoonlee@kriss.re.kr).

eliminated, and multiple steps are required to minimize the faults [1]. Hence, the sampling oscilloscope still seems the best solution for time domain analysis of high-speed pulses.

Broadband instruments such as VNAs and sampling oscilloscopes are generally supposed to measure signals at specified terminals having connectorized interfaces. In addition to such port-to-port analyses, in many cases, it is also important for system diagnosis to observe signals between ports. Although a mathematical method for this exists (called De-embedding) [2], on-wafer probe measurement has served as a standard method for genuine measurements, but it still contains inherent limitations such as bandwidth and coupling/invasiveness due to the nature of metallic tip use. To address this issue, we present an optical probing technique to realize significantly less invasive and advantageous measurement for higher bandwidth signal analysis in both the temporal and spectral domains. We implemented a ~ 20 GHz pulse generation/detection scheme in our sampling system to validate its spectro-temporal relations through commercial instruments, such as sampling oscilloscopes and electrical spectrum analyzers. In addition, the feasibility of the system as pulsed signal instrumentation is investigated through stability analysis. Finally, the losses and mismatches of a microstrip transmission line are extracted from the reflective pulses at the terminal port with various terminations.

2. OPTICAL SAMPLING SYSTEM FOR HIGH-SPEED PULSED SIGNALS

To break through the conventional challenges in electronic pulse measurement systems, the electro-optic (EO) sampling technique has become a viable solution [3–8]. Fig. 1 shows our EO system optimized for 20 GHz bandwidth signals. The system employs a femto-second-scale pulsed laser with ~ 0.1 ps duration and 80 MHz pulse repetition frequency (PRF). We split the pulses in half. One half of the pulses are used as an excitation beam to generate 20 GHz EM pulses through a fast photodiode. The other half of the pulses serve as an optical sampling beam which can be temporally overlapped with the EM pulses with a programmable delay line.

For an external EO sensor, we employed a minute x-cut $LiTaO_3$ tip as shown in Fig. 1(b). The sensor is vertically (z-direction) mounted along at the center of the transmission line. This is to effectively measure the normal electric field components of the EM pulses while they propagate along the line (y-direction) [9]. As the EM signal and optical sampling pulse (x-direction) reconcile in the EO sensor medium, the polarization of the original sampling pulse becomes modulated

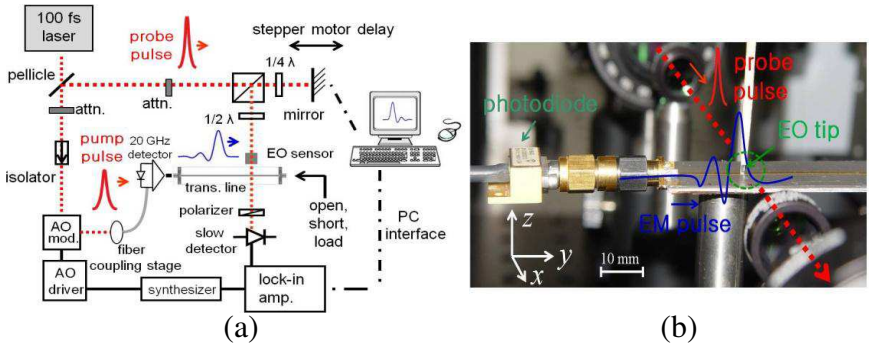

Figure 1. High-speed EM pulse measurement system based on electro-optic sampling, (a) overall system and (b) probing part.

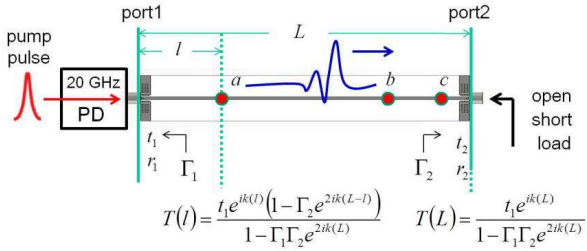

Figure 2. Signal transfer on a microstrip transmission line. (t, r, and Γ are the Fresnel and equivalent reflection field coefficient at each port. $T(l)$ denotes the transmission fields at location l.) (a, b and c are measurement points to be discussed.)

according to the electric fields of the EM pulses. This modulated polarization indicates the amount of EM-optical pulse interactions with respect to the temporal position of the sampling pulse. Translating the stepper motor in the sampling path, the sampling pulse can scan across the EM pulse. Thus, the original EM pulse waveform can be plotted on a computer screen by reconstructing the sampled trace.

3. TIME DOMAIN MISMATCH ANALYSIS WITH OPTICAL SAMPLING SYSTEM

We fabricated a wideband microstrip transmission line for 20 GHz signal transmission as illustrated in Fig. 2. The line is 200 mm long and designed to deliver up to 20 GHz signals. The generalized transmission

field at distance l from port1 is expressed as Eq. (1).

$$T(l) = \frac{t_1 e^{ik(l)} \left(1 - \Gamma_2 e^{2ik(L-l)}\right)}{1 - \Gamma_1 \Gamma_2 e^{2ik(L)}} \tag{1}$$

The transmission field $T(l)$ is an infinite geometric series in a closed-loop system including multiple reflections from both terminals. As port1 is well-matched with the source photodiode, Γ_1 can be considered negligible. Hence, the main field component at the arbitrary point l is re-expressed as $1-\Gamma_2 \exp(2ik(L-l))$. Note that the first term (i.e., 1) is the normalized incident pulse component, and the rest is the reflective term from port2. These two are the major field components that govern the both temporal and spectral responses over the transmission line at the points of interest.

Prior to measurement on a microstrip transmission line, we measured the output pulse from the 20 GHz photodiode using a commercial sampling oscilloscope (Tektronix: TDS8200). The output port of the photodiode was directly connected to the 2.4 mm coaxial measurement port of the oscilloscope. The measured pulse waveform is shown in Fig. 3(a), and this is to be the input pulse applied to port1 of the line.

The rising and falling times of the pulse are 10.0 ps and 12.5 ps, respectively. Such fast transition time corresponds to 28 to 35 GHz of a 3 dB bandwidth. In fact, the dashed line in Fig. 3(b) is the calculated spectrum of the pulse by the fast Fourier transform (FFT) algorithm. The spectrum basically matches well with the envelope of the spectrum measured by a commercial spectrum analyzer. (The spectrum is filled with 80 MHz of fine RF comb which is due to the PRF of the laser.) Both spectra degrade less than 3 dB at 20 GHz as expected.

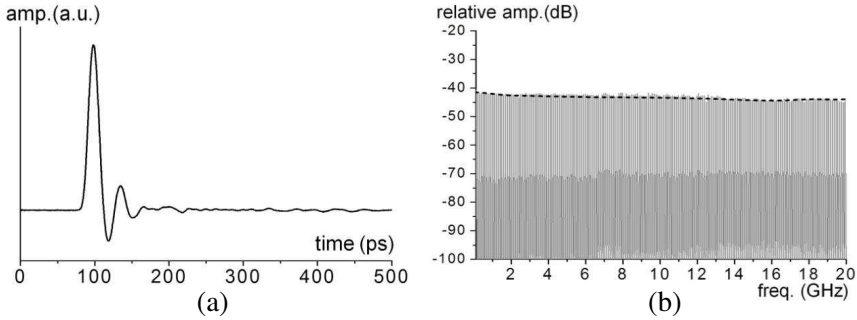

Figure 3. Response of a 20 GHz photodiode, (a) temporal response and (b) spectral response with FFT spectral envelope (dashed line).

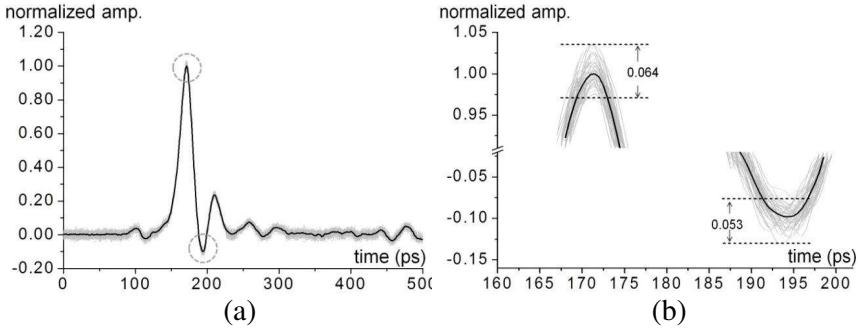

Figure 4. Pulse waveform at point a in Fig. 2, (a) normalized average waveform with 50 jitter traces and (b) detailed peaks circled in (a).

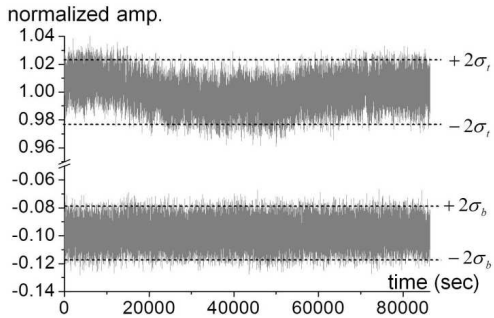

Figure 5. Stability of the pulse peak-to-peak distribution for 24 hours. (The dashed lines indicate 95% confidence level).

Verified from such pulse-spectrum transform and measurement by certified instruments, now we can measure spectro-temporal signals over the transmission line at arbitrary and portless points utilizing our EO system. First, we explored the pulse at a point 5 mm from port1 (point a in Fig. 2, $l = 5$ mm). Fig. 4 shows the 50 cumulative pulse traces (gray) at point a. A fast read-out time constant of a lock-in amplifier was used to grow pulse jitters and scrutinize them. The average pulse is normalized and shown as a solid line. Also, the detailed pulse deviations at the peak-peak and its average transition time are shown in Fig. 4(b).

Further statistical distributions of each peak are investigated in Fig. 5. Each trace is the typical evolution of each peak, collected every second for 24 hours (= 86400 sec). The 95% confidence interval of each

trace, associated with its respective sample standard deviation of top ($\sigma_t = 0.01156$) and bottom ($\sigma_b = 0.00964$) peaks, are presented. The top peak generally shows slightly larger deviation than the bottom case as it tends to have long term system drift. Noting that the σ_t and σ_b indicate the degree of fluctuation at each peak, such deviation affects the transition time of the pulse. In actuality, σ_t and σ_b are independent of each other; thus, they do not increase the standard deviation of the peak-peak ($\sigma_{p-p} = 0.01453$) significantly. This deviation corresponds to 2.65% of transition time (12.9 ps) error level with a 95% level of confidence.

The incident pulse changes its shape as it travels along the line. To observe the pulse waveform evolution, we measured the pulses at points 15 mm and 18 mm from port1 (points b and c in Fig. 2) with various terminations at port2. The pulse1–4, 2–5, and 3–6 are the respective cases of open, short, and 50-ohm terminations with a 2.4 mm calibration kit (Agilent: 85056A). Each pulse set is an averaged trace to reduce jitters and deviations as was done in Fig. 4. In all cases, the three primary incident pulses are identical, whereas their reflections are quite different for terminations.

The 1ns of swept timing was divided into three windows ($T1$, $T2$ and $T3$) based on discontinuities. $T1$ is the temporal window that shows the incident pulse heading to port2 before it gets reflected there. $T2$ shows reflection timing after the mild mismatch at the port2 connector before major reflection due to open (or short) terminations. The dominant reflective pulses are covered in the $T3$ window, including minor Fabry-Perot mismatches associated with port2 and open (or short) mismatches. The durations of $T1$, $T2$ and $T3$ can be changed by measuring at different points as shown in Figs. 6(a) and (b). The comparison of each window can be quite useful information regarding the transmission line. The waveforms of the primary pulses — compared to the launching pulse as in Fig. 3(a) — indicate lossy and dispersive characteristics of the line as the pulses propagate. For instance, the incident pulses at point b are less dispersive than those at point c as they are closer to the original pulse in Fig. 3(a), while the reflected pulses become more separated and attenuated as they travel further. In addition, the relative relations between primary and secondary (reflected) pulses — such as temporal separation, waveform broadening, amplitude contrast, and phase difference — heavily influence the spectral response of the pulses. This information should help to characterize the broadband transmission line by inferring the propagation constant from measurements such as the waveguide attenuation and the dispersion, etc.

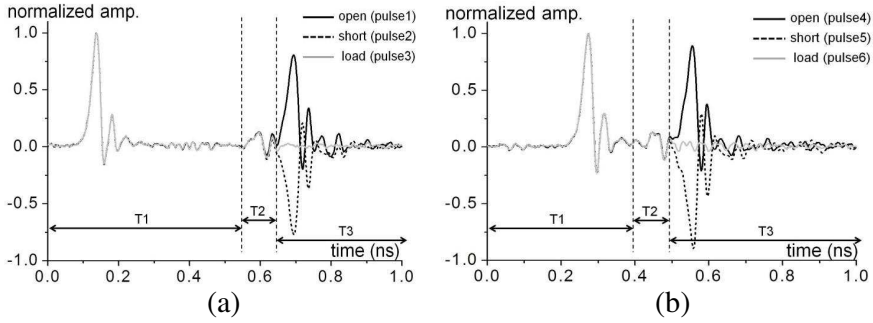

Figure 6. Pulse measurements with various terminations, (a) at point b and (b) at point c in Fig. 2.

4. FREQUENCY DOMAIN MISMATCH ANALYSIS WITH OPTICAL SAMPLING SYSTEM

The reflected pulses modulate the original spectra which are determined by the incident ones. Utilizing the verified pulse-spectrum transform technique, the extracted spectra from pulses in Fig. 6 are shown in Fig. 7. The relatively less dispersive primary pulses are in charge of the overall bandwidth. With respect to the primary pulse, the relative amplitude of the secondary pulse modulates the spectra mainly associated with their temporal separation and phase relation. As the reflective pulses from open (or short) termination have the same (or opposite) polarity with respect to the incident pulses, the pulses constructively (or destructively) build up at a very low frequency. Then, each open and short spectrum is modulated periodically in a complementary way for higher frequency. For 50-ohm termination cases, a mild 'open terminated' spectral modulation is observed due to the connector mismatch pulses as shown in the $T2$ windows of Fig. 6. Excluding such mismatch effect, the spectra for ideally matched termination such as the pulses in $T1$ windows of Fig. 6 are also presented in Fig. 7.

These incident pulses serve as reference channels as in a vector network analyzer. By normalizing Fig. 7 with respect to the incident pulses, the degree of mismatch can be re-scaled in Fig. 8. The ranges of spectral interference fringes indicate the degree of mismatch at the measurement point. Perfect matching ($VSWR = 1$) and full reflection ($VSWR = \infty$) yielded 0 dB and 6 dB of mismatch level in this analysis.

The mismatches are generally increased, whereas the echo signals are attenuated for higher frequency. The peaks of mismatches in Fig. 8

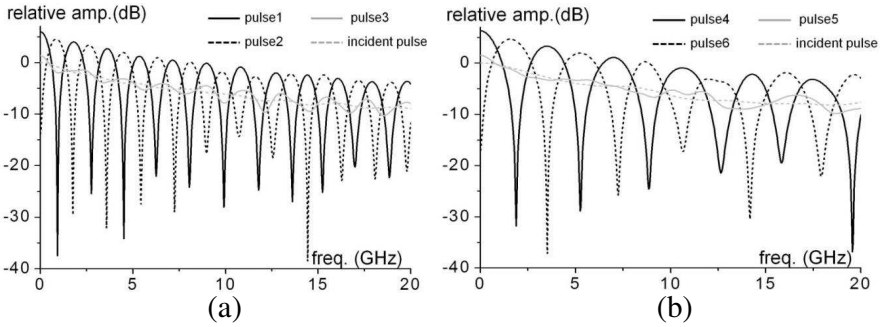

Figure 7. Spectral responses of the pulses in Fig. 6 by FFT (with relative dB scale), (a) for Fig. 6(a) and (b) for Fig. 6(b).

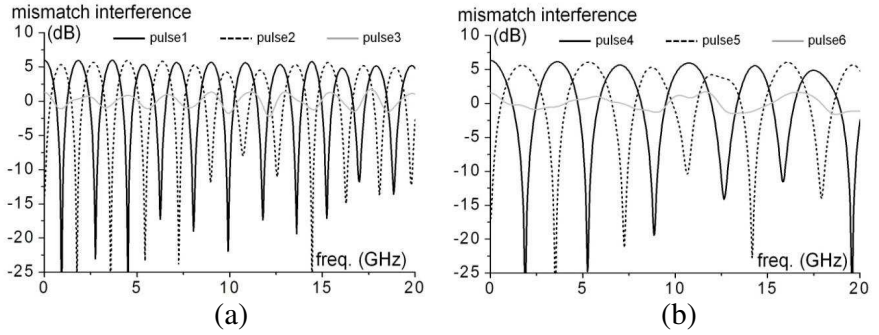

Figure 8. Spectral mismatch-interferences of the pulses in Fig. 6 by FFT (with relative dB scale), (a) for Fig. 6(a) and (b) for Fig. 6(b).

indicate that the reflection and attenuation are overall balanced for most of the 20 GHz band. In addition, the connector mismatches yield additional resonant effects associated with 'the deeper reflections' from the calibration kits. Such resonances between connector and port2 terminal result slight distortions in both spectra for open and short terminations, making them less complementary.

The connector mismatch can be exclusively extracted by considering only two pulses in the $T1$ and $T2$ windows. For instance, the mismatches which were in charge of modulation (due to pulse 3 in Fig. 8(a)) are re-plotted on the Smith chart as shown in Fig. 9. Its phase linearly shifts with frequency increase. This confirms that a single pulse is reflected back from the connector mismatch point without resonance.

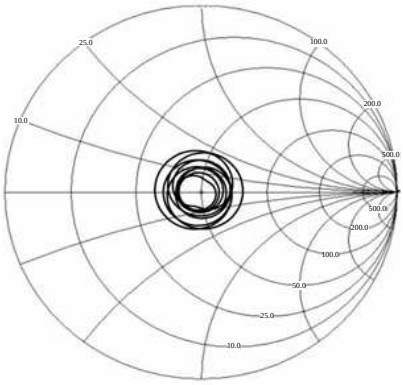

Figure 9. Connector mismatch trace up to 20 GHz at point b in Fig. 2.

5. CONCLUSION

A mismatch analysis method on a broadband transmission line, using a photonic-based sampling system, was presented. A portless optical probing scheme enabled measurement of trains of incident and reflected pulses at arbitrary locations on the signal line. By investigating the reflected pulses versus incident pulses, a temporal mismatch analysis including the characteristics of a line was carried out. These time domain results were also utilized for frequency domain analysis with an appropriate transform technique. Such an on-wafer probing system and reflectometry method can be a promising solution for the challenges in conventional electronic instrumentation.

ACKNOWLEDGMENT

This work is supported by Korea Research Institute of Standards and Science under the project of 'Establishment of National Physical Measurement Standards and Improvements of Calibration/Measurement Capability,' grant 12011002.

REFERENCES

1. Agilent Technologies, "Time domain analysis using a network analyzer," Application Note 1287-12, 2011.
2. Agilent Technologies, "De-embedding and embedding S-parameter networks using a vector network analyzer," Application Note 1364-1, 2009.

3. Valdmanis, J. A. and G. A. Mourou. "Subpicosecond electrooptic sampling: Principles and applications," *IEEE Journal of Quantum Electronics*, Vol. 22, No. 1, 69–78, 1986.
4. Frankel, M., J. F. Whitaker, G. A. Morou, and J. A. Valdmanis. "Ultrahigh bandwidth vector analyzer based on external electro-optic sampling," *Solid State Electronics*, Vol. 35, No. 2, 325–332, 1992.
5. Seitz, S., M. Bieler, M. Spitzer, K. Pierz, G. Hein, and U. Siegner, "Optoelectronic measurement of the transfer function and time response of a 70 GHz sampling oscilloscope," *Measurement Science and Technology*, Vol. 16, No. 10, L7–L9, 2005.
6. Williams, D. F., P. D. Hale, T. S. Clement, and J. M. Morgan, "Calibrated 200-GHz waveform measurement," *IEEE Trans. on Microwave Theory and Tech.*, Vol. 53, No. 4, 1384–1388, 2005.
7. Bieler, M., S. Seitz, M. Spitzer, G. Hein, K. Pierz, U. Siegner, M. A. Basu, A. J. A. Smith, and M. R. Harper, "Rise-time calibration of 50-GHz sampling oscilloscopes: Intercomparison between PTB and NPL," *IEEE Trans. on Instrum. Meas.*, Vol. 56, No. 2, 266–270, 2007.
8. Ma, Z., H. Ma, P. Gong, C. Yang, and K. Feng, "Ultrafast optoelectronic technology for radio metrology applications," *Journal of Systems Engineering and Electronics*, Vol. 21, No. 3, 461–468, 2010.
9. Lee, D. J. and J. F. Whitaker, "A simplified fabry-Pérot electro-optic modulation sensor," *IEEE Phot. Tech. Lett.*, Vol. 20, No. 10, 866–868, 2008.